34th Annual International Conference of the IEEE EMBS
San Diego, California USA, 28 August - 1 September, 2012

Interactive Segmentation of Airways from Chest X-ray Images using Active Shape Models

Teshwaree Tezoo and Tania S. Douglas, *Senior Member, IEEE*

Abstract— **Classification of airway shapes in chest X-ray images may be useful in computer-aided detection of lymphadenopathy associated with pediatric tuberculosis. This paper presents an interactive approach for airway segmentation from chest X-ray images that may be used in an airway shape classification algorithm. A local normalization filter is applied as a preprocessing step to enhance the visibility of the airways. Segmentation is then performed with the aid of active shape models (ASMs), which are warped to a set of manually defined control points on the image to be segmented, using an affine transformation. Two shape models are built, one of which consists of points on the airway edges only and the other consists of points on the airway edges as well as points on the ribs. The ASMs are built from a set of manually segmented images. The Hausdorff distance is used to compute the accuracy of the segmentations with reference to a manual segmentation.**

I. Introduction

Pulmonary tuberculosis (TB) caused an estimated 1.4 million deaths in 2010, according to the World Health Organization. The diagnosis often relies on chest X-ray imaging, especially in the case of children. Computer-aided diagnosis may be used to increase the accuracy of diagnosis and reduce the dependence on scarce radiologists, especially in low-income countries with a high TB burden.

Lymphadenopathy, which manifests as bronchial compression due to enlarged lymph nodes, is a hallmark indication of tuberculosis in pediatric pulmonary tuberculosis [1]. X-ray images contribute to the resources used for the detection of lymphadenopathy because of easy access and low cost as well as the lower radiation exposure in comparison with computed tomography [3]. A study carried out by Swingler et al. [3] concluded that the use of chest X-ray imaging to detect lymphadenopathy in children is unreliable due to the poor visibility of airways. However, digital slot scanning radiography has been shown to provide better visualization of airways compared to the image quality provided by conventional X-ray systems [4]. It may be possible to exploit the airway visibility in such images to aid the diagnosis of diseases such as TB which lead to changes in the shape of chest airways.

Research supported by Lodox Systems and the Technology and Human Resources for Industry Programme of the National Research Foundation in South Africa.

Teshwaree Tezoo is an MSc student in the Biomedical Engineering Programme and the MRC/UCT Medical Imaging Research Unit, University of Cape Town.

Tania S. Douglas is with the Biomedical Engineering Programme and the MRC/UCT Medical Imaging Research Unit, University of Cape Town, Observatory 7925, South Africa. (phone: +27 21 4066541; fax: +27 21 4487226; e-mail: tania@ieee.org).

The lack of contrast between overlapping anatomical structures in chest X-ray images renders the airway borders inconspicuous. Therefore, low-level segmentation methods which rely on local pixel intensity, such as threshold, region growing or edge detection are ineffective for accurate shape delineation. Model based segmentation methods may be used, as they can overcome detection limitations due to shape variations among airways and low contrast. In this paper we describe the use of interactive segmentation of airways using active shape models (ASM). The aim is to delineate the airway edges for potential use in the classification of airway abnormalities caused by TB-induced lymphadenopathy in children.

II. Methodology

Fig. 1 shows the steps involved in segmenting the airways. To obtain delineated airway shapes, test images are initially filtered using a local normalization filter followed by warping of a mean airways model to the airways, and finally segmentation by the ASM algorithm.

A. Local normalization filter

The local normalization filter performs global equalization of contrast throughout an image [5]. It normalizes the local image intensity difference from the local average based on the local standard deviation. The local normalization of an input image L can be described as follows [5]:

$$L_{LN} = (L - L_G)/((L^2)_G - (L_G)^2)^{1/2} \qquad (1)$$

where L_{LN} is the local normalization filtered image and subscript $_G$ indicates Gaussian blurring. The only parameter in this equation is the standard deviation of the Gaussian blur, which determines the size of the region used in calculating the local mean and standard deviation. Experiments were performed by Long [2] to determine the optimum local normalization filter width to be used in relation to the average maximum airway diameter. A filter width of 80% the average maximum airway diameter was found to be optimal for segmentation methods based on relative greyscale intensities, such as ASM. The maximum airway width was measured each of all the images in a training set and the average was calculated. 80% of this average value was used as filter width.

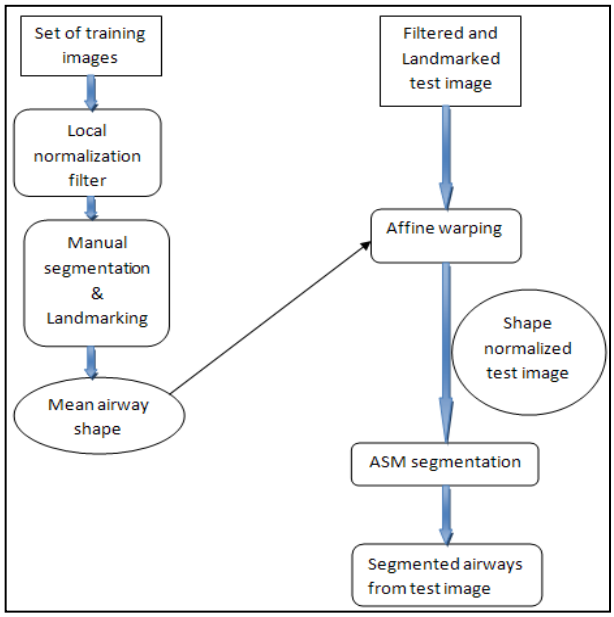

Figure 1. Steps involved in interactive segmentation using ASM

B. *Interactive active shape model segmentation*

Active shape model (ASM) segmentation was first developed by Cootes et al. [6]. It builds statistical models of a particular object's shape and grey-scale landscape by using a set of annotated training images in which a set of key landmark points have been marked. The point distribution model (PDM) and the local image intensity are then calculated around each of those landmark points [6].

1) *Building the shape model*

The shapes from the manually segmented training set of X-ray images first need to be normalized to filter out the effects of pose (position, scale and rotation) to provide a true representation of the shape of an object. Procrustes analysis can be used to align the shapes and obtain a mean object shape. The Procrustes distance is a computation based on least-squares differences between landmarks comprising the shapes, to remove the effect of translation, rotation and scaling. The shape model is built as follows [7]:

a) The centroids of a set of shapes are determined.

b) The shapes are aligned with respect to position at their centroids.

c) The mean shape is computed through the following iterative algorithm:

i. The first shape in the training set of images is established as an approximate mean shape.

ii. The remaining shapes are aligned to the approximate mean to minimize the Procrustes distance.

iii. The approximate mean shape is re-calculated from the aligned shapes.

iv. Steps ii and iii are repeated until the mean shape converges on a stable shape.

d) The shape component for every instance in the training set is computed as the difference between the mean shape and the pose normalised shape for that particular instance.

At this stage the point distribution model is used to record the statistics of these aligned shapes by modeling the co-dependent variation of the landmark points.

Principle component analysis is then applied to the aligned set of images Ut to represent it by the mean shape ū, the eigenvalues (λ1, λ2,. . ., λk) and the corresponding eigenvectors (q1, q2,…, qk). The first t eigenvectors are selected, Q = (q1, q2,…, qt), such that the shape vector ui can be approximated as follows [7] :

$$u_i \approx \bar{u} + Q_i \qquad (2)$$

where i = (i_1, i_2,..., i_t) is the vector of weights which controls the variants of the mean shape $\bar{u}$ of ASM.

The gray-level appearance of the object is modelled by examining the gray-level profiles obtained in the normal direction to the shape at each landmark point. Statistical analysis of these profiles is used to create a model for each landmark that consists of the mean gray-level profiles and its modes of variation [6].

2) *Image search*

Given a rough starting position, the active shape model can be fitted to a test image. An iterative approach to fit the shape model to a test image is as follows [6]:

a) Examine a region of the image around each landmark point to calculate the displacement required to move it to a better location.

b) Compute the adjustments to the pose and shape parameters in accordance to the displacements.

c) Update model parameters by enforcing limits on the shape parameters. Global shape constraints can be applied to ensure that the shape of the model instance remains similar to those in the training set.

A. *Comparing segmented shapes*

The Hausdorff distance measures the extent to which each point on one shape lies near some point of another shape and vice versa, when the two shapes are superimposed over one another [9]. This shape comparison method is suitable for instances where not all points from one shape have a corresponding point on the other, due to occlusion and noise. In such cases, where the two point sets are of different sizes so that no one-to-one correspondence exists between all points, the Hausdorff distance provides a dissimilarity measure [10].

The Hausdorff distance haus is defined as follows:

$$haus = \max (\max_i d(a_i, B), \max_j d(b_j, A)) \qquad (3)$$

where, i= 1,…,m; j = 1,…,n,

A = {a1, a2,…, am}: the semi-automatically segmented airways to be evaluated, B = {b1, b2,…, bn }: the airways against which the semi-automatically segmented airways is to be evaluated. Each ai or bj is a point on the airway edge.

$$d(a_i,B) = \min_j \| b_j - a_i \| \quad (4)$$

where, $j = 1, \ldots, n$.

III. Experiments And Results

The chest radiographs used for this study were obtained using the Lodox Statscan slot scanning digital radiography machine on healthy and suspected TB patients at the Red Cross Children's Hospital in Cape Town. 31 chest X-ray images were used for the training set, 14 of which were from healthy individuals and 17 from paediatric TB patients. A set of 25 images was used to test the performance of the algorithm, 14 of which were from healthy individuals and 15 from paediatric TB patients.

To improve the visibility of the airways in the radiographs, all the images were first filtered using the local normalization filter. Fig. 2 shows the filter results.

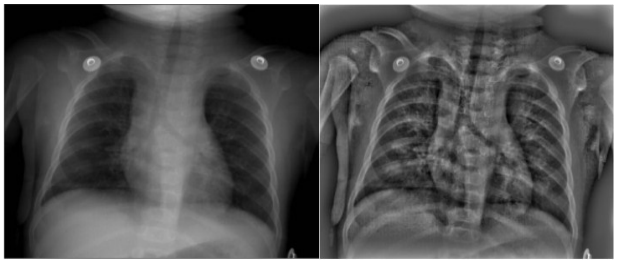

(a) Original image (b) Filtered image

Figure 2. Application of local normalization filter.

Convergence of the shape model to the desired object depends heavily on algorithm initialization and the selected landmark points. To handle the lack of reliable landmark points on the airway structure, we built two different shape models. Comparison of the segmentation resulting from each of them would indicate which one is a better initialization for the ASM segmentation algorithm. One of the models is built from labeled points and landmarks on the airways only, while the other is built from points on the airways as well as the ribs. Each image in the training set was manually annotated with 30 points on the airway edges, 9 of which were used as control points, and 8 points on the ribs. All of the labeled points on the ribs as well as the 9 control points on the airways were used to build the shape model that uses airways and rib points. Only the 9 control points from the airway edges were used to build the shape model based on airway points only. The remaining manually annotated points were used as manual segmentation to test the performance of the segmentation algorithms. The airway shape to be segmented is restricted to the first bifurcation only since the visibility of the structure is significantly poor for further branching of the airways. Fig. 3 illustrates the control points used for the models.

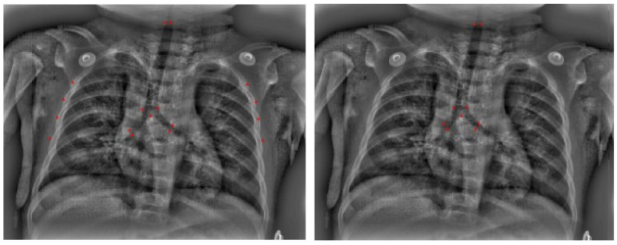

(a) Airway and rib points based (b) Airway points based

Figure 3. Landmark points for the two shape models

Each model was initialized by warping the corresponding shape model to the test image using an affine transformation. Landmark points were manually selected on the test image to which the mean shape was warped. Fig. 4 shows the warped mean models for a particular test image, while Fig. 5 shows the ASM segmentation resulting from each shape model. In Fig. 4(a) the warped shape model constitutes of the mean airway model as well as the 8 rib points, which are also used as landmark points to guide the ASM segmentation algorithm. However in Fig 4(b) the warped shape model constitutes of the mean airway model only.

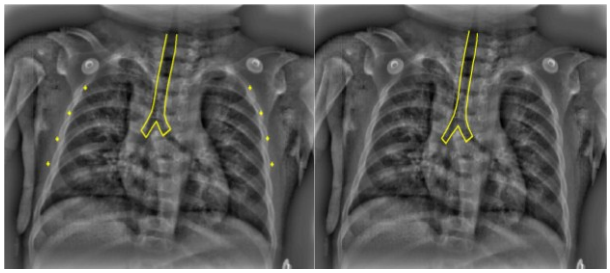

a) Airway and rib points based (b) Airway points based

Figure 4. Affine warping results for the two shape models.

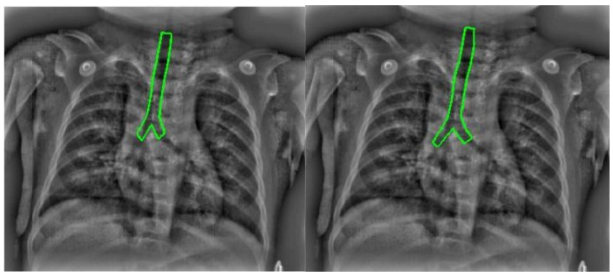

a) Airway and rib points based (b) Airway points based

Figure 5. ASM segmentation results for the two shape models.

As a means to determine the matching accuracy of the two models, the Hausdorff distance was used. For each image, the manually segmented airway shape was used as ground truth. Fig. 6 shows a typical manual segmentation. The Hausdorff distance between the manually segmented airways and the segmentation output from the initialization with the shape model built from airway points only, as well as from airway and rib points, was calculated for each image in the test dataset of 10 images. Table 1 shows the Hausdorff

distance statistics as an indication of how dissimilar the ASM segmentations are to the manual segmentation.

TABLE I. HAUSDORFF DISTANCE STATISTICS (IN PIXELS) FOR ASM MODELS

	Mean	**STD**
Airway points model	18.89	9.94
Airway & rib points model	25.18	15.67

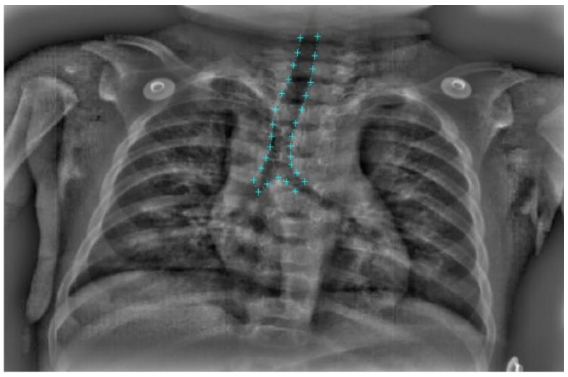

Figure 6. Manual airway segmentation

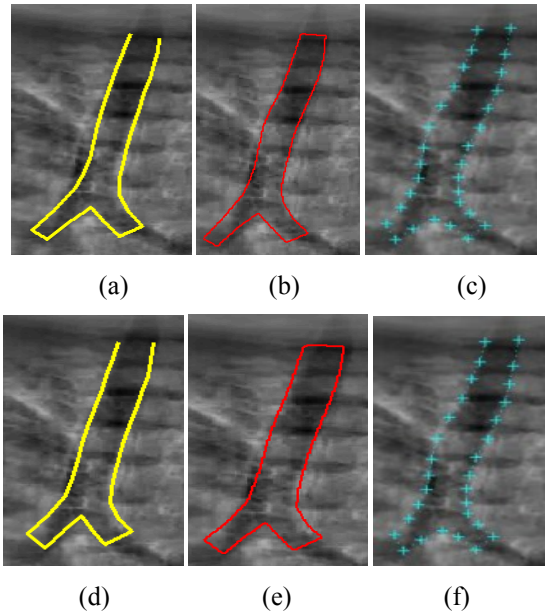

Figure 7. Segmentation results; top row: airway points based model; bottom row: airway and rib points based model; yellow: affine warping of shape model to manually selected points; red: ASM segmentation; blue: manual segmentation.

IV. CONCLUSION

This paper presents an interactive way of segmenting airways from X-ray images using active shape models. Initialization, which is one of the key contributors to a good segmentation, is performed by warping a mean shape model onto a test image, with the aid of control points selected manually.

The airways were successfully delineated with the interactive ASM algorithm using both shape models. The Hausdorff distance comparison shows that the shape model built from airway and rib points produces greater variation and less similarity to manual segmentation that the model built from airway points only. The airways-only model requires less user interaction.

The segmentation methods may be used in studies to determine whether the segmented airways of TB-infected children differ significantly in shape from those of healthy children. If they do, the airway segmentation algorithms may have potential for use in an airway classification tool for the detection of lymphadenopathy associated with tuberculosis in children.

REFERENCES

[1] S. Andronikou & N. Wieselthaler, "Modern imaging of tuberculosis in children: thoracic, central nervous system and abdominal tuberculosis," *Pediatric radiology.*34(11):861-875, 2004.

[2] M.Long, "Segmentation of full body regions and airways in full-body digital paediatric X-ray images," Master's thesis, University of Cape Town, 2008.

[3] G. Swingler, G. Du Toit, S. Andronikou, and others, "Diagnostic accuracy of chest radiography in detecting mediastinal lymphadenopathy in suspected pulmonary tuberculosis," *Archives of Disease in Childhood.* 90(11):1153, 2005.

[4] R.D. Pitcher, A.B. van As, V. Sanders, et al, " A pilot study evaluating the "STATSCAN" digital X-ray machine in paediatric polytrauma," *Emergency Radiology.*15(1):35-42, 2008.

[5] A.M.R. Schilham, B. Van Ginneken & M. Loog, "A computer-aided diagnosis system for detection of lung nodules in chest radiographs with an evaluation on a public database," *Medical image analysis.* 2006. 10(2):247-258.

[6] T.F. Cootes, C.J. Taylor, D.H. Cooper, J. Graham, " Active shape models–their training and application," *Computer Vision and Image Understanding*.1995. Vol 61,pp.38–59.

[7] M.B. Stegmann, "Active appearance models - theory, extensions and cases," Technical University of Denmark 2000.

[8] M. Pantic, L. Rothkrantz, "Facial action recognition for facial expressionanalysis from static face images," IEEE Transactions on Systems, Man, and Cybernetics, Part B, 2004, vol. 34, no. 3, pp. 1449-1461.

[9] D. P. Huttenlocher, G.A. Klanderman & W. Rucklidge, W, "Comparing images using the hausdorff distance," *IEEE Transactions on Pattern Analysis and Machine Intelligence*. 1993. 850-863.

[10] R. C. Veltkamp, " Shape matching: Similarity measures and algorithms," 2001. *Smi,*0188